Heliyon 9 (2023) e20840

Contents lists available at ScienceDirect

Heliyon

journal homepage: www.cell.com/heliyon

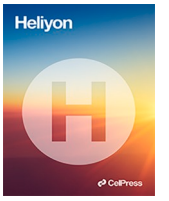

Experimental study on the thermal performance of ultra-thin flat heat pipes with novel multiscale striped composite wick structures

Menghao Wang [a,1], Yinchuang Yang [c,1], Yiwei Sun [d], Jian Li [a,b,**], Menglong Hao [a,b,*]

[a] Key Laboratory of Energy Thermal Conversion and Control of Ministry of Education, School of Energy and Environment, Southeast University, Nanjing, 210096, PR China
[b] National Engineering Research Center of Power Generation Control and Safety, School of Energy and Environment, Southeast University, Nanjing, 210096, PR China
[c] Department of Mechanical and Aerospace Engineering, The Hong Kong University of Science and Technology, Clear Water Bay, Kowloon, Hong Kong SAR, PR China
[d] School of Materials Science and Engineering, Southeast University, Nanjing, 210096, PR China

ARTICLE INFO

Keywords:
Ultra-thin flat heat pipe
Striped composite wick
Multiscale
Thermal resistance

ABSTRACT

The rapid development of power-intensive and flexible electronic devices requires thinner heat-dissipation devices with better thermal performance. Ultra-thin flat heat pipe (UTFHP) with striped wick structure is a promising candidate for this application, but its wick structure and thermal performance have not yet been thoroughly studied and optimized for the small concentrated heat source, which is commonly encountered in electronics. In this study, several concentrated striped composite wick (CSCW) structures for 0.6 mm thick UTFHPs are proposed and experimentally investigated. The CSCW consists of copper foam with striped passages converging in the heating zone and double layers of copper screen mesh. The thermal performance of UTFHPs with various composite wick structures is experimentally evaluated. UTFHPs with the proposed structures are also compared with a UTFHP with a more conventional parallel passage composite wick structure. Experimental results show that the CSCW with the hollow structure at the evaporation section is preferred, due to the directed liquid working medium reflux and a large vapor-liquid evaporation interface. Besides, the passage width of the copper foam significantly affects the thermal performance. With the best-performing wick structure, the UTFHP gives the lowest thermal resistance of 0.79 °C/W at a heat load of 23.34 W. Its effective thermal conductivity is approximately 7 times that of copper. The proposed striped wick structure for UTFHPs provides an alternative to handle the hot-spot challenge of electronic devices.

1. Introduction

As microelectronics and information technology have advanced rapidly recently, many electronic devices are moving towards

* Corresponding author. Key Laboratory of Energy Thermal Conversion and Control of Ministry of Education, School of Energy and Environment, Southeast University, Nanjing, 210096, PR China.
** Corresponding author. Key Laboratory of Energy Thermal Conversion and Control of Ministry of Education, School of Energy and Environment, Southeast University, Nanjing, 210096, PR China.
E-mail addresses: eelijian@seu.edu.cn (J. Li), haom@seu.edu.cn (M. Hao).
[1] Authors contributed equally.

https://doi.org/10.1016/j.heliyon.2023.e20840
Received 20 July 2023; Received in revised form 16 September 2023; Accepted 9 October 2023
Available online 10 October 2023

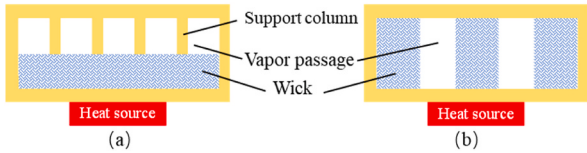

Fig. 1. The arrangement of wick and vapor passage: (a) layered structure; (b) striped structure.

miniaturization [1], high integration, and high performance [2]. Accordingly, the power required and the heat flux generated by electronic devices, such as high intensity light-emitting diode (LED) [3], electric vehicle batteries [4,5], and power amplifiers [6], will continue increasing significantly in the future. Consequently, electronic devices are faced with serious thermal management challenges. To meet these requirements, the heat dissipation module must be lightweight, compact, and have excellent heat dissipation capability. Conventional cooling methods using water, air, and other working mediums for forced convection cooling are unsuitable due to their bulky size and complicated structure [7]. These cooling methods are also challenging to implement in portable electronics. Hence, alternative cooling techniques are necessary to fulfill these cooling requirements. Flat heat pipe (FHP), which transfers considerable amounts of heat by effectively employing the phase change circulation of working medium, emerges as a promising solution for meeting the challenge. It has the advantages of low thermal resistance, small volume, no external energy cost [8,9], and the ability to establish effective thermal contact with the surface of a planar heat source, such as computer and mobile phone central processing units (CPUs) which generate local area heat concentration. Thus, it becomes an important tool for addressing the current hot-spot problem of power-intensive electronic devices within a confined space.

FHP with a thickness of a few millimeters or more is no longer suitable for the thermal management of rapidly iteratively updated microelectronic systems. Therefore, the ultra-thin flat heat pipe (UTFHP) with an overall thickness below 2.0 mm has become an important research direction currently [10]. Researchers have proposed various kinds of UTFHPs and made attempts to optimize their performance. Ding et al. [8] created a 30 mm × 30 mm × 0.6 mm (length × width × thickness) titanium-based UTFHP by using laser welding technology, rendering a maximum heat transfer power of 7.2 W. Oshman et al. [11] proposed a 1 mm thick polymer-based FHP which could operate at 11.94 W in the horizontal state. Later, they produced another 1.31 mm thick polymer-based FHP with a wick consisting of three layers of sintered copper mesh [12]. The thermal resistance of a copper reference sample with the same size was 4.6 times that of the UTFHP. Lewis et al. [13] designed a 0.5 mm thick flexible UTFHP. Double-layer copper mesh and electroplated copper columns functioned as the wick and vapor passage, respectively. The UTFHP could function at a heating power of 8 W. Although polymer-based UTFHPs have good flexibility and lightweight properties, they also face issues including the release of non-condensable gas from the polymer and low thermal conductivity. Xu et al. [14] presented a 0.28 mm thick UTFHP with a composite wick structure comprised of a layer of stainless-steel mesh and an array of micro copper columns. At a power of 7.9 W, an effective thermal conductivity of 1398 W/(m·K) was obtained. Lee et al. [15] fabricated a 0.91 mm thick UTFHP. The wick consisted of single-layer copper mesh, while the vapor passage was formed by three layers of coarse copper mesh. The ultimate heat load was about 5.4 W under the horizontal unbent condition. Huang et al. [16] proposed five 1.26–1.7 mm thick UTFHPs using solder paste soldering. Double-layer coarse copper mesh and single-layer fine copper mesh worked as the vapor and liquid passages, respectively. The heat dissipation power in the horizontal direction was 50 W (the heat source size: 20 mm × 20 mm). Chen et al. [17] produced a 0.4 mm thick UTFHP with a maximum heat transfer capacity (HTC) of 4.5 W at the horizontal position by designing the wick with a 300 in^{-1} copper mesh and the support for vapor passage with a micro-pillar array. Yang et al. [9] studied the heat transfer performance of UTFHP with a new type of wettability pattern for evaporators. Li et al. [18] suggested a 2 mm thick UTFHP with bionic grading microchannels. The UTFHP could endure a thermal load of 24 W at the optimum inclination angle. The thermal performance of UTFHPs is improved by using different shell materials, wick structures, and manufacturing processes. However, the maximum heat transfer capacity of UTFHP with a relatively thin thickness is still not very excellent.

From the above literature review, the overall dimensions of UTFHPs, especially the thickness, can significantly impact the heat transfer capacity. Most of the above-mentioned studies adopted a layered structure for UTFHPs, whose wick and vapor passage are separated in the thickness direction, as shown in Fig. 1(a). The performance of UTFHPs with a layered structure can be strengthened by the optimization of wick structure, but it also brings some problems in the development of UTFHPs. UTFHPs with a layered structure achieve ultra-thinness by reducing the thickness of the vapor or liquid chamber, which increases the vapor flow resistance and inhibits liquid reflux. These effects lead to a considerable decrease in critical heat flow density, greatly deteriorating the thermal performance of the UTFHPs. On the other hand, UTFHPs with a layered structure of vapor and liquid flowing in opposite directions have a high vapor friction coefficient [19], leading to a high pressure drop and a low maximum heat flux. Therefore, UTFHPs with a striped structure as shown in Fig. 1(b) have been proposed [2,20]. In the striped structure, the wick and vapor passage are assembled in the same plane. The porous wick functions as a self-supporting and fluid pumping. Additional support columns are not needed, reducing the overall thickness and production complexity. Moreover, this type of wick structure gives a lower vapor spreading resistance at the adiabatic section of UTFHP when compared with a layered-structure UTFHP of the same thickness, because of the lower vapor passage wall surface area. Lv et al. [21] used a five-layer super-hydrophilic sintered screen mesh cut into a striped structure as the wick to create a 100 mm × 50 mm × 0.95 mm UTFHP. The parallel and rectangular vapor passages were processed by wire electrode cutting. The experimental results showed that the minimum thermal resistance was 0.039 °C/W. Zhou et al. [20] proposed a 0.8 mm thick UTFHP that utilized a hybrid wick structure that sintered copper foam and screen mesh together. The UTFHP withstood a maximum heat load of 5 W at an optimal filling ratio of 100 %. Subsequently, they fabricated six 0.75 mm thick striped UTFHPs with composite

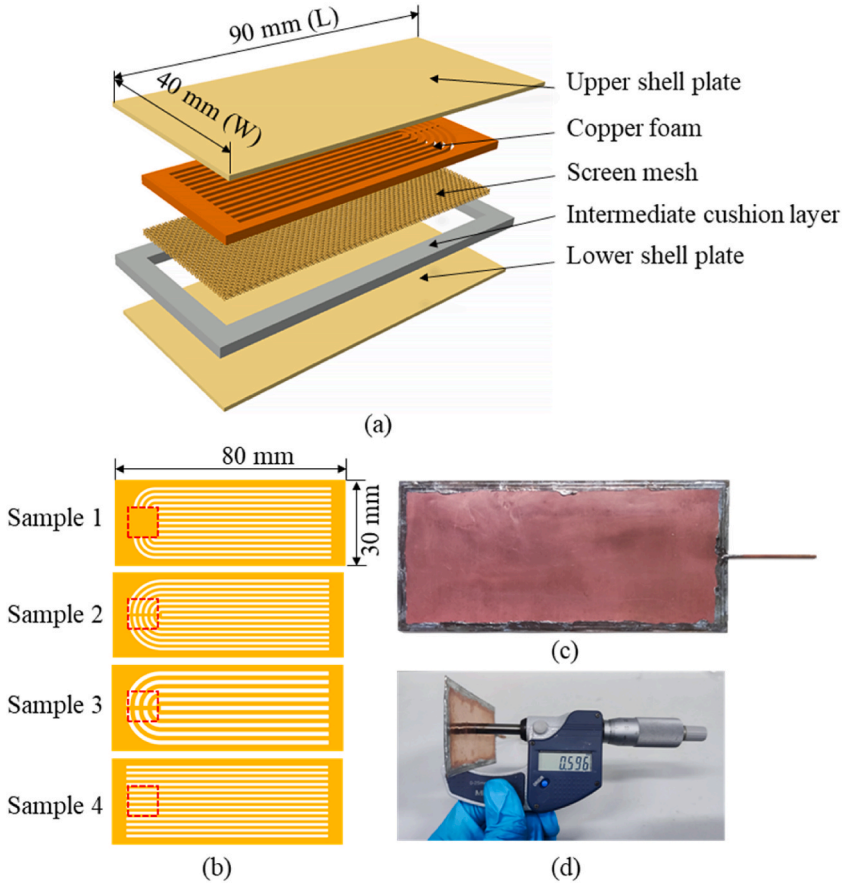

Fig. 2. Schematic of the UTFHP: (a) internal structure configuration of UTFHP; (b) different wick structures (the red dotted frame is the heating zone); (c) assembled sample of UTFHP; (d) thickness of UTFHP.

wick structures of different widths [22]. The influence of the vapor-liquid passage space allocation percentage on the thermal characteristics of UTFHPs was investigated. It was found that the optimal area ratio of UTFHPs was 67.28 % with a maximum heat load of 8.5 W (a heated zone of 15 mm × 9 mm in size). Li et al. [23] proposed a UTFHP with a thickness of less than 0.5 mm and a striped wick structure consisting of sintered screen mesh. The phase-change process and two-phase flow in the striped wick were studied by visualization, and it was found that the striped wick structure can alleviate the two-phase counterflow well. Huang et al. [24] designed a 100 mm × 15 mm × 0.5 mm UTFHP with a striped structure. The wick consisted of six spiral woven wire mesh layers and a bottom layer of screen mesh, with a maximum input heating power of 10.5 W (heat flux of 4.67 W/cm^2) in the gravity position. Cui et al. [25] presented a 105 mm × 50 mm × 0.68 mm UTFHP with a striped sintered screen mesh wick structure. The wick was thermally oxidized to enhance capillary force. The UTFHP could withstand 8 W (on a 1 cm^2 heating area) with a minimum thermal resistance of 0.26 °C/W.

So far, relatively little research has been done on UTFHPs with a striped structure. Research on UTFHPs with a striped structure mainly focuses on optimizing the arrangement of vapor-liquid passages and trying different types of wick and surface treatments to improve heat transfer performance. The wick structure and thermal performance have not yet been thoroughly studied and optimized for the small concentrated heat source. The striped structure can achieve a higher heat transfer capacity, but some challenges need to be solved first. Some striped UTFHPs are created by flattening cylindrical copper heat pipes [20,22]. Restricted thickness and simple shape may limit its applications. The other striped UTFHPs are made by welding and sealing two thin plates with a wick structure [21,24,25]. The vapor and liquid passages are relatively single in structure and designed with parallel structure at the evaporation section. However, when the parallel passage structure is faced with a small concentrated heat source such as CPU, the liquid pumped by the parallel passage wick on both sides of the heat source needs to be transported to the heating zone again, resulting in a long reflux path. Moreover, fewer vapor transport passages can be used efficiently, and the overall thermal performance is not excellent. Solving these challenges in enhancing the thermal performance of UTFHPs with a striped structure is the goal of our research.

Therefore, this paper presents UTFHPs with novel striped composite wick structures. The thickness of UTFHPs is 0.6 mm, and their heat transfer characteristics are studied experimentally. The composite wick comprised of copper foam and screen mesh meets the requirements of high permeability and capillary force. The axially concentrated striped structure made at the evaporation section of the copper foam can provide more available passages for vapor transport and realize the directed backflow of liquid working fluid to

Table 1
Detail parameters of different UTFHP samples.

Sample	Vapor passage width (mm)	Liquid passage width (mm)	Vapor passage number	Liquid passage number	Screen mesh number
SP1	1	1	13	12	500
SP2	1	1	13	12	500
SP3	1.5	1.5	9	8	500
SP4	1	1	13	12	500

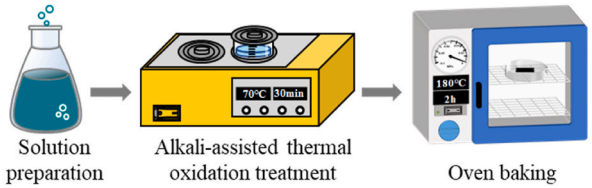

Fig. 3. Preparation process of super-hydrophilic micro/nanostructures.

the heating zone. Multiscale micro/nanostructures are prepared on the surface of the wick to make it super-hydrophilic, thus improving the capillary force and pumping the working medium more rapidly. The influence of filling ratio, heat load, wick structure, and passage width on the thermal performance of UTFHPs proposed are experimentally investigated.

2. Experimental setup and theory

2.1. Design and manufacture of the UTFHP

The overall structure of the proposed UTFHP consisted of an upper shell plate, an intermediate cushion layer, a lower shell plate, and a composite wick comprised of copper foam and screen mesh. The internal structure configuration of the UTFHP is illustrated in Fig. 2(a). The UTFHP had an overall external size of 90 mm × 40 mm and an internal functional area of 80 mm × 30 mm. The upper and lower shell plates were both fabricated from 80 μm thick copper foil. The intermediate cushion layer was composed of a 400 μm thick copper plate, providing space for the wick placement. The composite wick comprised 130 in^{-1} copper foam with a thickness of 300 μm and a double-layered 500 in^{-1} copper screen mesh with approximately 160 μm in total thickness. The copper foam served both as the vapor passage and the wick structure. Because the intersection layer in the wick can enhance the evaporation rate and the backflow ability of the wick [26], the double-layered mesh acted as the additional wick structure to maintain the working circulation. The mesh layers and the foam structure were held together by the vacuum force applied by the shell plates. Electroplating bonding [13] and diffusion bonding [27] were possible methods to reduce interlaminar thermal contact resistance and further improve thermal performance. As depicted in Fig. 2(b), striped vapor passages with different shapes and widths were fabricated in the copper foam using laser die cutting. The remaining part of the copper foam formed a strip-shaped wick, assisting in the backflow of the condensed liquid to the heating zone. This configuration realized vapor-liquid separation and weakened the interaction between them. Independent and efficient transport passages for vapor and liquid in the heat pipe are guaranteed.

To investigate how the geometrical parameters of the configuration affect the heat transfer characteristics of UTFHPs, four various types of copper foam structures were designed, as depicted in Fig. 2(b). Sample 1 contained a square concentrated evaporation zone on the wick that served as an evaporator. Sample 2 and Sample 3 had a similar structure with concentrated striped passages at the evaporation section, but they differed in the width of the passage. Compared with Sample 1, Sample 2 and Sample 3 were designed to be partially hollow at the evaporation section. The above three structures all had divergent vapor passages to improve the utilization of passages for vapor transport. The liquid passages converged to the concentrated heating zone to fully utilize the liquid pumping capacity of the wick. A configuration composed of parallel passages was also designed to demonstrate the advantage of the proposed configuration, as illustrated in Sample 4. It is worth mentioning that the copper foam structure at the left of the heating zone can serve as a compensation chamber, storing liquid working medium to delay dry-out. The wick with a vapor passage width of less than 1 mm was difficult to machine. When the vapor passage width was greater than 1.5 mm, it was hard to ensure good support for the shell plate. As a result, this study concentrated primarily on the experimental results of the passage width of 1 mm and 1.5 mm.

Fig. 2(c) shows the physical diagram of the manufactured UTFHP. Sn/Ag/Cu (96.5/3/0.5) solder was used to seal the gap between the upper/lower shell plate and the middle cushion layer. A copper tube with a diameter of 0.8 mm was inserted at the right end of the UTFHP mainly for evacuation and working medium injection. A gap in the edge of the intermediate cushion layer provided space for the copper tube to be inserted. Degassed deionized water was preferred for the working medium. Water was the most used working medium for copper-based heat pipes because of its high latent heat of vaporization and surface tension [28,29]. The degassing and deionization of the working medium can reduce the influence of non-condensable gas and prevent electrochemical corrosion, respectively. As demonstrated in Fig. 2(d), the overall thickness of the UTFHP was about 0.6 mm. Details of different UTFHP samples geometric parameters are summarized in Table 1.

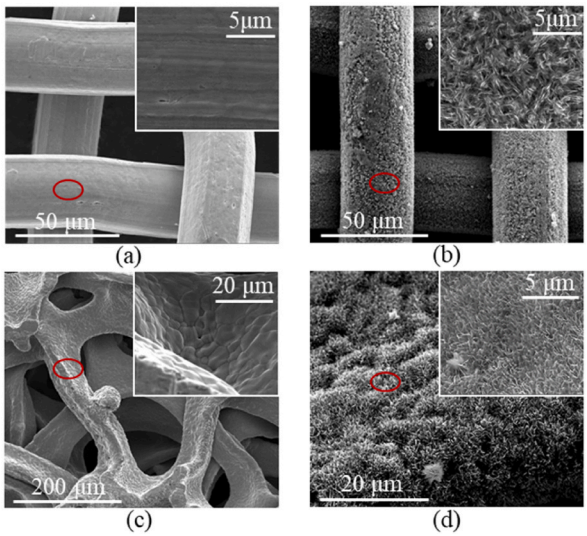

Fig. 4. SEM photographs of wick structures: (a) bare screen mesh; (b) micro/nanostructured screen mesh; (c) bare copper foam; (d) micro/nanostructured copper foam.

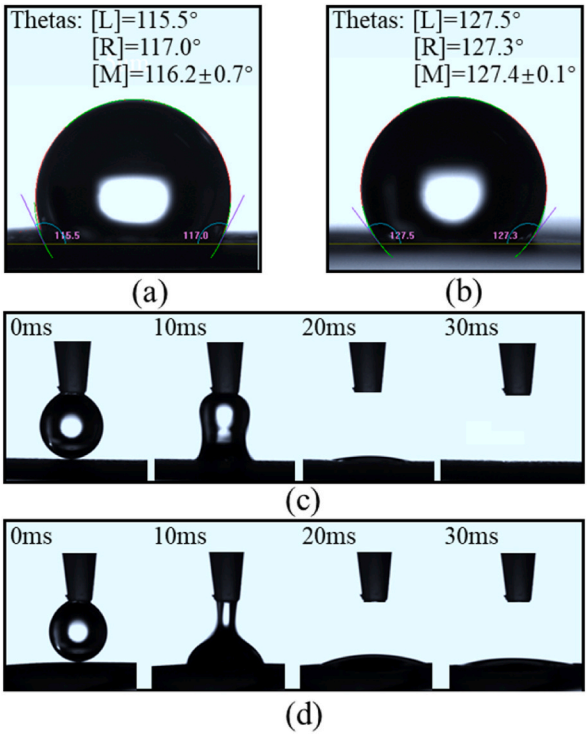

Fig. 5. The wettability test of screen mesh and copper foam: static contact angle of bare copper foam (a) and bare screen mesh (b); the penetrating process of a 3 μl water drop on the micro/nanostructured copper foam (c) and micro/nanostructured screen mesh (d).

2.2. Fabrication of multiscale micro/nanostructured wick

It has been suggested that the multiscale micro/nanostructured wick improves the heat transfer performance of UTFHP through the enhancement of capillary force and increased evaporation rate [26,30]. Thus, blade-like nanostructures were formed and almost covered the outside surface of copper foam/mesh to produce the multiscale micro/nano wick structure in this work. Alkali-assisted thermal oxidation was utilized to fabricate the super-hydrophilic multiscale micro/nanostructured wick [31]. The preparation procedures are depicted in Fig. 3. First, a mixed solution of 0.065 mol/L $K_2S_2O_8$ and 2.5 mol/L KOH was prepared. The cleaned screen

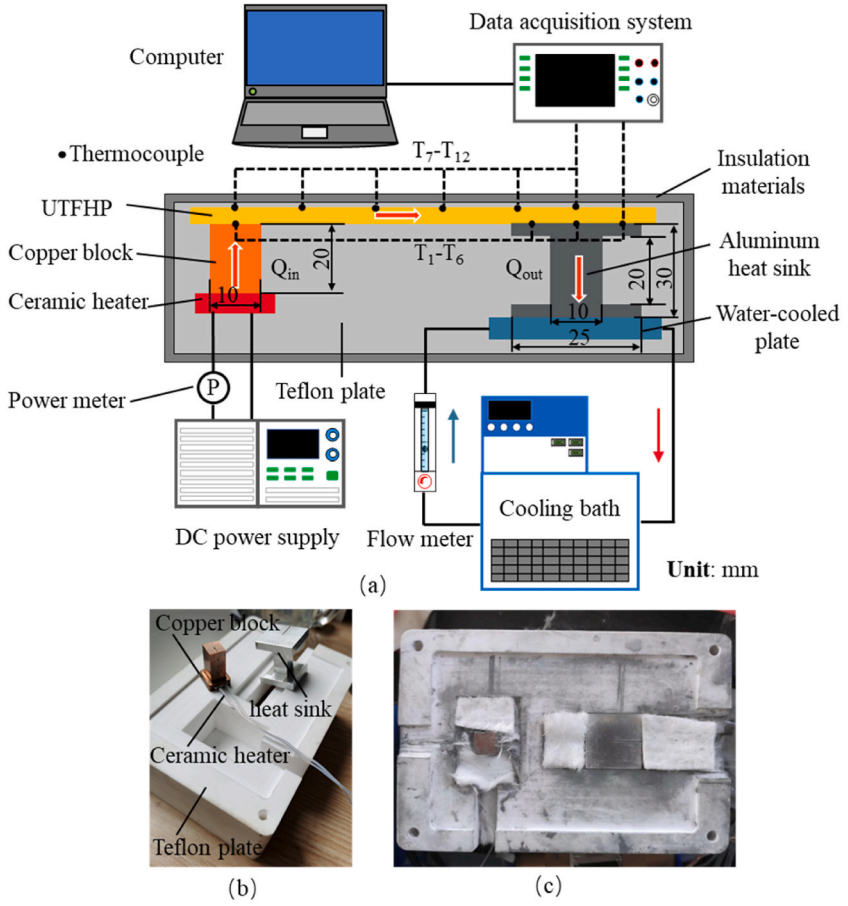

Fig. 6. Diagram of the experimental testing system: (a) experimental setup; (b) partial components; (c) assembly.

mesh and copper foam were subsequently immersed in the mixed solution, and the reaction was carried out at a temperature of 70 °C for 30 min. Next, the screen mesh and copper foam were cleaned with deionized water. The final procedure was to regulate the oven temperature to 180 °C and bake the cleaned materials for 2 h. Fig. 4 is a SEM diagram of the surface morphology of wick before and after oxidation treatment. The surface characteristics of screen mesh/copper foam changed considerably after oxidation. The surface of the wick structure was relatively smooth before oxidation, as indicated in Fig. 4(a) and (c). After oxidation, blade-like nanostructures were formed on the surface, leading to an increase in roughness, as depicted in Fig. 4(b) and (d). As a result, the thin-film evaporation area became enlarged and the capillary force increased [7]. Fig. 5 shows the wettability test results of deionized water in the wick. The static contact angles of copper foam and screen mesh before the micro/nanostructures fabrication process were 116° and 127°, respectively, as displayed in Fig. 5(a) and (b). The formation of micro/nanostructures significantly enhanced the hydrophilicity of the wick such that the measurement of contact angle became difficult. The water droplets were almost attached to the surface before the oxidation process. However, a complete wetting by a water droplet was observed on the surfaces after oxidation (Fig. 5(c) and (d)). The droplets dispersed quickly and subsequently spread into the copper foam and the screen mesh, indicating strong super-hydrophilicity of the wick.

2.3. Experimental setup and uncertainty analysis

The experimental platform depicted in Fig. 6(a) was established to test and estimate the thermal performance of UTFHPs. The entire experimental platform mainly included four components for heating, cooling, data acquisition, and thermal insulation, respectively. The heat was generated by a ceramic heater powered by a DC power supply (Keithley 2260B-80-27, 0.01 W resolution). The input heating power varied between 2.60 W and 26.36 W. The copper block with cross-sectional dimensions of 10 mm × 10 mm and a height of 20 mm conducted heat from the ceramic heater to the evaporation section of the UTFHP, as shown in Fig. 6(b). The

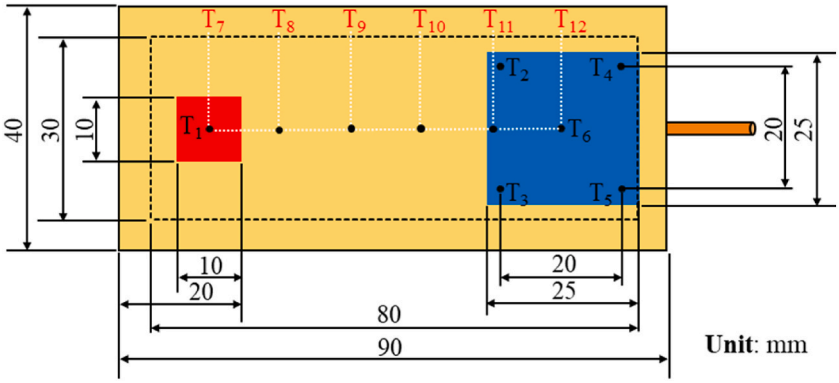

Fig. 7. Position distribution of thermocouples on the surface of UTFHP.

ceramic heater, DC power supply, and copper block constituted the heating module. The heat was then effectively transferred to the condensation section by the UTFHP and rejected at the condensation section to an aluminum heat sink under a water-cooling module. The aluminum heat sink, water-cooled plate, constant temperature circulating water tank, and flowmeter made up the cooling module. The size of the top and bottom surface of the aluminum heat sink was 25 mm × 25 mm, and the cross-section size of the middle part was 10 mm × 10 mm. The temperature stability of the circulating water tank was 0.1 °C. A flow meter was employed for regulating and recording the flow rate of the circulating liquid through the water-cooled plate. The temperature of the circulating water tank was programmed to 25 °C and the flow rate was regulated to 1.8 L/min. The data acquisition module was used for recording the temperature-characteristic data on the surface of the UTFHP. It consisted of several K-type thermocouples (the accuracy: 0.1 °C), a laptop, and a data acquisition instrument (Keithley DAQ6510). The acquisition frequency was set to 1/5 Hz. A thin layer of thermally conductive silicone grease with 6 W/(m·K) rated thermal conductivity was applied to the interface between the UTFHP and the heated copper block/aluminum heat sink to lower the contact thermal resistance. Additionally, the whole apparatus was insulated with Teflon block and aerogel to minimize heat loss both through radiation and convection during testing, as shown in Fig. 6(c). The UTFHP was subjected to a uniformly distributed constant pressure of about 98 N to ensure full contact with the heater and condenser blocks during the test.

To estimate the thermal performance of UTFHPs, the thermocouples were tightly affixed to the surface of UTFHP with their specific position distribution shown in Fig. 7. T_1, located on the evaporator, was used for the measurement of the evaporation section temperature T_e. T_2-T_6, located on the condensation section, were used to evaluate the condensation section temperature T_c, which is defined by Eq. (1):

$$T_c = \frac{T_2 + T_3 + T_4 + T_5 + T_6}{5} \tag{1}$$

T_1-T_6 were located on the bottom surface of the UTFHP. T_7-T_{12}, uniformly located on the central axis on the top surface of the UTFHP, were applied to monitor the temperature distribution. With known evaporation section temperature T_e, condensation section temperature T_c, and the input heat load Q, we can evaluate the thermal performance of UTFHP by using an effective total thermal resistance, which is calculated by Eq. (2):

$$\mathrm{R} = \frac{T_e - T_c}{Q} \tag{2}$$

At atmospheric pressure, the thermal performance of UTFHPs at various filling ratios was investigated in the horizontal state. The filling ratio is expressed as **Eq. (3)** [20]:

$$\eta = \frac{V_l}{V_p} \times 100\% \tag{3}$$

where V_l and V_p are the volume of liquid working medium and pores within the composite wick, respectively. When the UTFHP reached steady state, the temperature of measurement points was recorded and utilized for calculating the thermal resistance. The temperature was measured 20 times and averaged to reduce the uncertainty of the measurement. The steady state is determined when the temperature changes of all thermocouples exceed no more than 0.5 °C within 5 min.

The uncertainty analysis was carried out by the comprehensive method of relative error analysis [32]. The relative uncertainty of the thermal resistance is determined by the following Eq. (4) [33]:

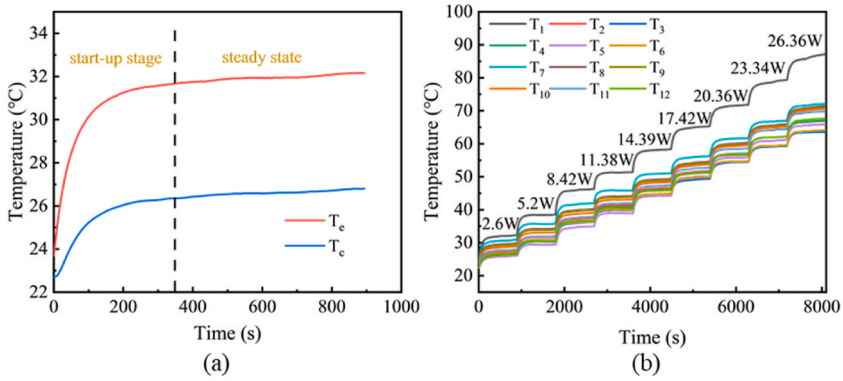

Fig. 8. Thermal response characteristics of UTFHP: (a) start-up performance; (b) operating characteristic.

$$\begin{aligned}\frac{\delta R}{R} &= \frac{\sqrt{\left(\frac{T_e - T_c}{Q^2}\cdot\delta Q\right)^2 + \left(\frac{\delta T_e}{Q}\right)^2 + \left(\frac{\delta T_c}{Q}\right)^2}}{\frac{T_e - T_c}{Q}} \\ &= \sqrt{\left(\frac{\delta Q}{Q}\right)^2 + \left(\frac{\delta T_e}{T_e - T_c}\right)^2 + \left(\frac{\delta T_c}{T_e - T_c}\right)^2} \\ &= \sqrt{\left(\frac{\delta Q}{Q}\right)^2 + \left[\frac{\delta(T_e - T_c)}{T_e - T_c}\right]^2}\end{aligned} \tag{4}$$

When the heating power is 2.60 W, SP2 at a filling ratio of 111.4 % is used to analyze the maximum relative uncertainty of thermal resistance. Considering the error of data acquisition, the measurement uncertainty of temperature is calculated to be 0.12 °C. The power meter accuracy is 0.01W. The surface temperature of the insulation at maximum heating power (26.36 W) was measured to estimate the heat loss. The results showed that the surface temperature was about 27 °C. The ambient temperature was 25 °C. The heat loss is estimated to be about 1.0 W according to the formula of natural convection and heat radiation. It is no more than 3.79 % of the heating power. Therefore, the maximum relative uncertainty of the thermal resistance computed by the above method is 4.51 %.

3. Results and discussion

3.1. Thermal response characteristics of UTFHP

The thermal response characteristics of the UTFHP are analyzed first. As illustrated in Fig. 8(a), sample SP2 with a 111.4 % filling ratio is selected to illustrate the typical thermal response of the UTFHP. It is observed that the temperature rises quickly in the first 100 s of the start-up stage. Then, the rising speed decreases significantly, and the temperature gradually levels off. After about 350 s, the temperature fluctuation of the thermocouple is less than 0.5 °C, meaning that the UTFHP succeeds in starting and reaches a steady state. The thermal response time indicates the time required from the beginning of the heat load change until the UTFHP reaches the next steady state. Fig. 8(b) demonstrates the operating characteristic of SP2 at various heat loads. The temperature at each measurement point rises as the increase in heat load. The temperature difference between the adiabatic section and the condensation section (T_c) at all heat loads is relatively small. However, as the heat load continuously increases, the temperature difference between the evaporation section (T_e) and other sections enlarges considerably. In addition, the UTFHP reaches steady state after a period at a constant heat load. The temperature of the UTFHP can also quickly regain steady state when the heat load is changed.

3.2. Temperature distribution of UTFHPs

As presented in Fig. 9, the surface temperature of the UTFHP samples SP1 (Fig. 9(a)), SP2 (Fig. 9(b)), SP3 (Fig. 9(c)), and SP4 (Fig. 9(d)) at various filling ratios varies with the input heat load. At a small heat load, the surface temperature of UTFHPs exhibits good uniformity. Besides, the temperature difference between T_e and T_c remains at a relatively low level. As the input heat load increases, the absolute temperature as well as the temperature difference between T_e and T_c of UTFHP samples gradually rise. The large temperature difference between T_e and T_7 at a large heat load indicates the appearance of dry-out. Besides, the surface temperature distribution of UTFHP samples is also impacted by the filling ratio. When the input heat load is small, the filling ratio has little impact on the temperature difference between the evaporation and condensation sections. However, when the heat load increases to certain extent and approaches the dry-out limit, the temperature difference at different filling ratios differs dramatically. For example, the temperature differences of SP1 between T_e and T_c at 94.7 %, 111.4 %, and 128.1 % filling ratios reach 5.9 °C, 5.8 °C, and 6.1 °C, respectively, when the input heat load is 2.6 W. While the input heat load continues to increase to 23.34 W, the temperature differences

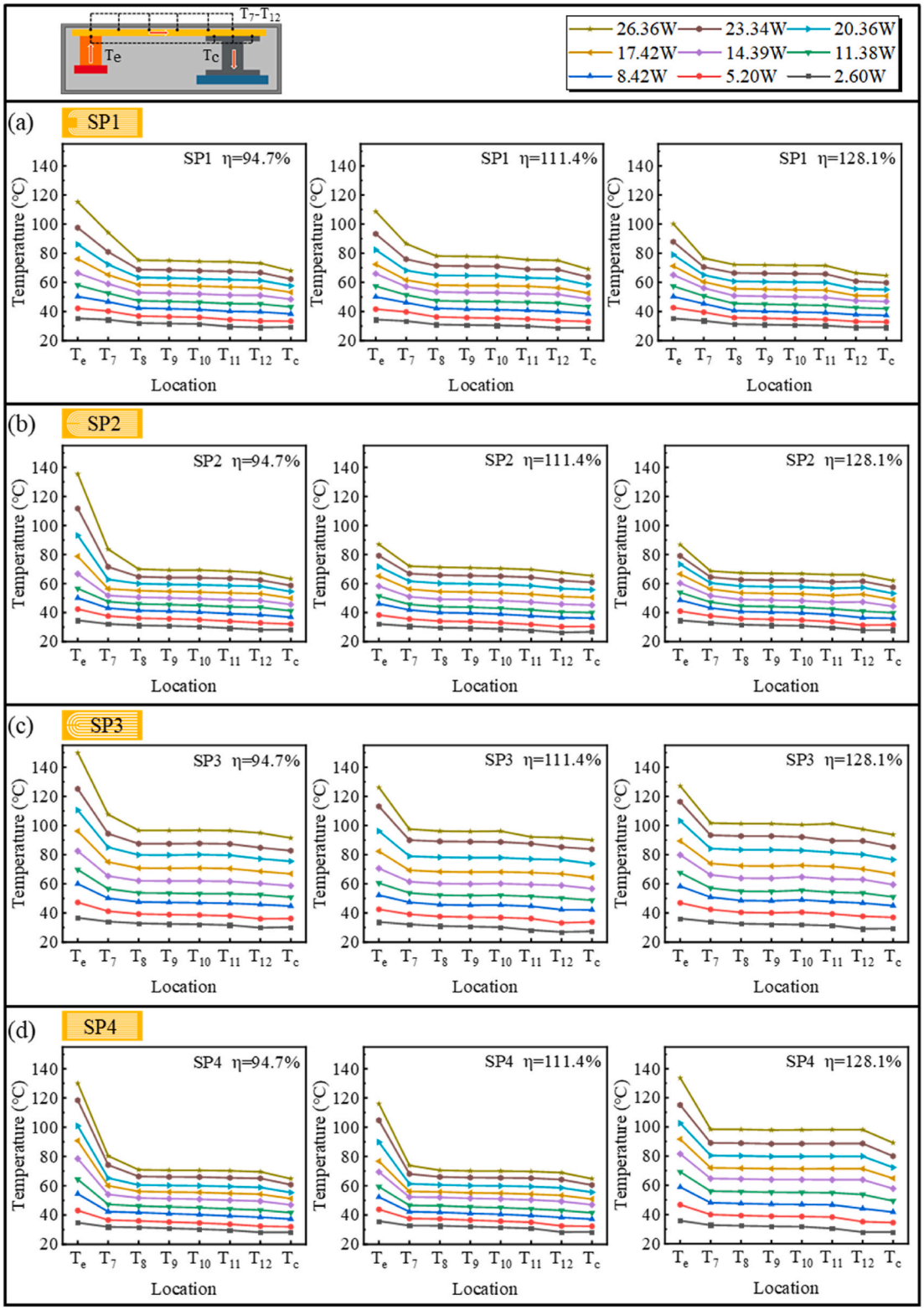

Fig. 9. Temperature distribution of UTFHPs at different filling ratios: (a) SP1; (b) SP2; (c)SP3; (d) SP4.

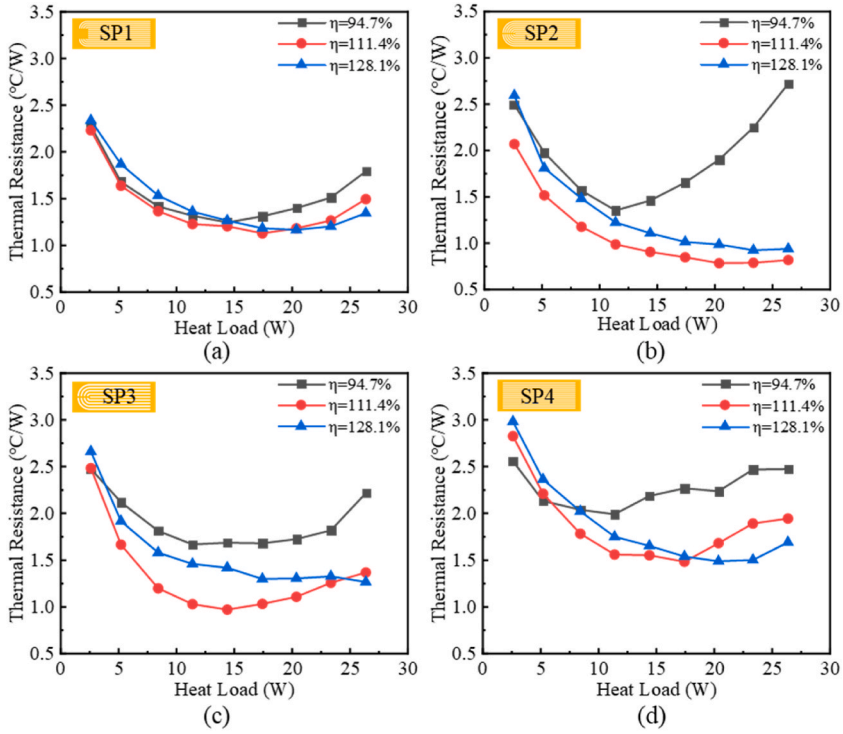

Fig. 10. Thermal resistance of UTFHPs at different filling ratios: (a) SP1; (b) SP2; (c)SP3; (d) SP4.

reach 35.3 °C, 29.6 °C, and 28.1 °C, respectively, indicating a better ability to pump liquid to participate in vapor circulation at a higher filling ratio. Moreover, when the input heat load is 26.36 W, the temperature differences between T_e and T_c of SP1, SP2, SP3, and SP4 at a 94.7 % filling ratio reach 47.2 °C, 72.1 °C, and 58.4 and 65.2 °C, respectively. A clear decrease in temperature difference is observed as the filling ratio increments to 111.4 % and 128.1 %. Especially for SP2, the temperature differences are only 21.6 °C and 24.8 °C. The temperature difference between the evaporation and condensation sections of the UTFHP sample at a large input heat load is reduced by increasing the filling ratio. The reason is that the UTFHP sample with a low filling ratio has less working medium participating in the heat transfer circulation. The evaporation section tends to dry out easily when a great deal of heat cannot be transported to the condensation section promptly. The other reason is that the liquid working medium may undergo superheating and form nucleate boiling on the surface of the evaporation section at a sufficiently large input heat load [20,34]. The bubbles are likely to be confined within the porous wick and hard to escape, thereby increasing the evaporation resistance and obstructing the circulation of the working medium. The temperature of the evaporation section stays at a high level. Therefore, when the input heat load is large, the temperature difference at a low filling ratio is more significant than that at a large filling ratio. The filling ratio should be increased appropriately to delay dry-out and enhance the thermal performance of UTFHP at a large heat load.

3.3. *Thermal resistance of UTFHPs*

The overall thermal resistances of UTFHPs SP1, SP2, SP3, and SP4 at different filling ratios are evaluated according to **Eq. (2)**, with the results shown in Fig. 10(a), (b), (c), and (d), respectively. Generally, as the input heat load increases, the thermal resistance of UTFHP samples initially decreases and then increases. For instance, the thermal resistance of SP1 at the 94.7 % filling ratio drops rapidly from 2.28 °C/W to 1.25 °C/W when the input heat load increases from 2.60 W to 14.39 W. The thermal resistance gradually increases to 1.79 °C/W when the input heat load increases from 14.39 W to 26.36 W. The evaporation rate of the liquid working medium at a small heat load is slow, resulting in a thick liquid film on the vapor-liquid interface at the evaporation section. Heat is transferred through the liquid film by heat conduction. The low thermal conductivity of the liquid working medium leads to high thermal resistance at the evaporation section. An increase in heat load intensifies the evaporation process and enhances the evaporation rate, thus lessening the liquid film thickness which provides more space for the vapor. In addition, when the heat load increases, the intense evaporation occurring at the evaporation section leads to the receding of the liquid meniscus into the wick. The meniscus radius difference between the evaporation and condensation sections at the vapor-liquid interface increases, which improves the capillarity of the wick and accelerates the cycle speed of the working medium [33]. Therefore, the heat transfer process in the UTFHP is further enhanced and the thermal resistance is decreased. A further increase in heat load disrupts the previous flow pressure balance of the working medium, due to the limitation of wick reflux capacity. Dry-out occurs locally at the evaporation section and the dry-out

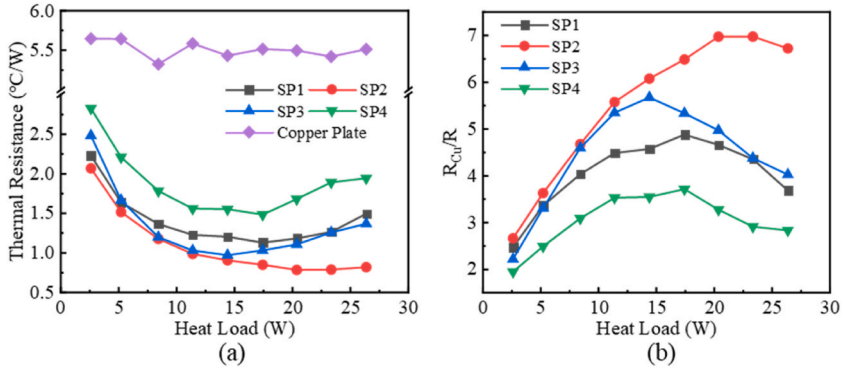

Fig. 11. Comparison of the thermal resistance of UTFHPs at the optimal filling ratio: (a) comparison of the thermal resistance of UTFHPs and copper plate; (b) the ratio of the average thermal resistance of the copper plate to the thermal resistance of UTFHPs.

regions expand with the increase in heat load. Lack of sufficient liquid working medium to participate in the vapor circulation results in increased thermal resistance.

The filling ratio has a significant impact on the thermal performance of UTFHP, especially the thermal resistance and HTC. For a given UTFHP sample, the increment of filling ratio causes a growth in the heat load corresponding to the occurrence of minimum thermal resistance (the maximum HTC). For example, the minimum thermal resistance of SP3 at 94.7 %, 111.4 %, and 128.1 % filling ratios are 1.66 °C/W, 0.97 °C/W, and 1.29 °C/W, and the corresponding input heat loads are 11.38 W, 14.39 W, and 17.42 W, respectively. The insufficient liquid supply of UTFHP samples with a low filling ratio leads to locally drying out easily at a small heat load. Increasing the filling ratio can delay the appearance of dry-out, thereby improving the maximum HTC. It is worth noting that at the high filling ratio (128.1 %), the maximum HTC of SP1, SP2, SP4, and SP4 can reach about 20 W. However, the thermal resistance at the 128.1 % filling ratio is generally higher than that at the 111.4 % filling ratio. The reason is that the liquid film at the vapor-liquid interface of the evaporation and condensation sections is thick at a high filling ratio, which causes large evaporation thermal resistance and condensation thermal resistance. In addition, the high filling ratio leads to a reduction in the available vapor flow space, which conversely brings about an increase in flow resistance and a more significant vapor pressure drop. Consequently, the thermal resistance of the UTFHP increases and the thermal performance deteriorates. The optimal filling ratio refers to the filling ratio that minimizes the thermal resistance under all experimental conditions of UTFHP. The optimal filling ratio for all UTFHPs is 111.4 % since the minimum thermal resistance is gained at the filling ratio for all types of UTFHP. The maximum heat transfer capacities of SP1, SP2, SP3, and SP4 at the optimal filling ratios are 17.42 W, 23.34 W, 14.39 W, and 17.42 W, respectively.

3.4. Influence of wick structure

To examine how the wick configuration affects the thermal performance of UTFHPs, the thermal resistance of various UTFHPs at the optimal filling ratio is compared, as indicated in Fig. 11(a). Besides, the thermal resistance test results of a same-sized copper plate are given. The average thermal resistance of the copper plate is 5.51 °C/W. The thermal resistance of the copper plate hardly changes at varying heat loads and is significantly higher than that of the four types of UTFHP samples because it transfers heat through heat conduction. When the heat source is small and concentrated, SP4 with a traditional parallel passage structure has the worst thermal performance, with a minimum thermal resistance of 1.48 °C/W. SP2 and SP3, which are designed to be partially hollow at the evaporation section and have a concentrated striped passage structure, perform better in thermal performance. The minimum thermal resistance of SP2 and SP3 is 0.79 °C/W and 0.97 °C/W, respectively. SP1 also has a concentrated striped passage structure. The difference is that it has a bulk copper foam structure at the evaporation section. SP1 has a minimum thermal resistance of 1.13 °C/W which is higher than that of SP2 and SP3, but lower than that of SP4. Fig. 11(b) shows the ratio of the average thermal resistance of the copper plate to the thermal resistance of UTFHPs. The thermal resistance of the copper plate is about 4.9, 7, 5.7, and 3.7 times that of the UTFHP SP1, SP2, SP3, and SP4, respectively.

Compared with SP4, SP1 has a 44 % reduction in minimum thermal resistance. The reason for the better performance of SP1 is that when the heat source is concentrated, the axially concentrated striped passage structure designed at the evaporation section can provide more available passages for vapor, which is beneficial to reduce evaporation resistance and improve vapor transport efficiency [22]. Moreover, the structure realizes the directed backflow of liquid working medium to the heating zone, reducing the flow pressure drop. However, only a few parallel vapor passages of SP4 can be utilized in the heating zone, resulting in a low vapor transport efficiency and large evaporation resistance. In addition, due to the concentration of the heat source, the liquid working medium pumped by the parallel passage wick on both sides of the heating zone needs to be transported to the heating zone again [23], leading to a long backflow path and significant flow pressure drop. Therefore, the thermal performance of the axially concentrated striped passage configuration is better than that of the parallel configuration when facing a small concentrated heat source. It is observed that SP2 has the lowest minimum thermal resistance and can bear a 26.36 W heat load with a negligible increase in thermal resistance. SP2 exhibits

Table 2
Comparison of the thermal performance with other works.

References	Thickness (mm)	Q_{max} (W)	K_{eff}/K_{Cu}
Li et al. [33]	2	120	5
Chen et al. [17]	0.43	4.5	–
Lewis et al. [13]	0.5	8	3
Cui et al. [25]	0.68	8	–
Huang et al. [24]	0.51	10	–
Previous work [26]	0.53-0.6	22.66	5.5
Present work	0.6	23.34	7

a reduction of around 30 % in minimum thermal resistance as compared to SP1. The reason is that the bulk copper foam structure of the concentrated evaporation zone at the evaporation section of SP1 leads to a relatively small area for the vapor-liquid interface where evaporation occurs, increasing the evaporation thermal resistance [34]. Besides, nucleate boiling likely occurs at the evaporation section when the input load is sufficiently large. The bulk copper foam structure brings about a longer escape path of vapor bubbles and a larger evaporation thermal resistance. As shown in Fig. 9, the temperature difference between T_e and T_7 of SP2 at the filling ratio of 111.4 % is less than that of SP1, which also indicates that the thermal resistance of evaporation decreases.

Since SP2 exhibits superior thermal performance, SP3 is designed with a similar structure to SP2 for investigating the influence of passage width on thermal characteristics. The copper foam of SP3 is designed with a 1.5 mm width for both the vapor passage and the liquid passage. However, SP3 presented worse thermal performance than SP2 when the vapor passage width is increased to 1.5 mm, whether it is analyzed from the maximum HTC or the minimum thermal resistance. It is not quite consistent with the previous research in reference [25]. In their opinion, when the vapor passage is narrow, the vapor flow velocity is large, resulting in great vapor flow resistance and liquid-vapor counterflow resistance. Moreover, when the vapor flow velocity is relatively high, the inertia effect is noticeable and the possibility of liquid entrainment inside is relatively high. These factors jointly reduce the circulation efficiency of the working medium. Based on our research findings, it can be concluded that the augmenting of the vapor passage width does not reduce the total thermal resistance. The possible reason is that SP2 has more passages, which creates a larger vapor-liquid interface area at the evaporation and condensation sections. This characteristic is beneficial for increasing the evaporation rate and condensation rate of the working medium, leading to a reduction in the evaporation thermal resistance and condensation thermal resistance. The improvement of the evaporation and condensation process has a more pronounced positive impact on thermal performance. The decrease of the maximum HTC of SP3 may be due to the compression of the vapor chamber during the evacuation process, which causes the increase of vapor pressure drop. However, the deformation of the shell plate cannot be seen macroscopically. Thus, the width of the vapor passage should be designed reasonably on the premise of ensuring the full support of the shell plate, and the interface area between the evaporation and condensation sections should be increased to improve thermal performance.

3.5. Comparison with other works

To further evaluate the thermal performance of UTFHP in this work, the test results of other literature works in the horizontal direction are given, as shown in Table .2. Although the UTFHP proposed by Li et al. [33] can withstand 120 W heat load, it is thick and the effective thermal conductivity compared with copper is not very high. In other literature works [13,17,24,25], the UTFHP with a thickness close to this work can only withstand less than 10 W. On the whole, the UTFHP we designed in this work can withstand higher heat load, and the effective thermal conductivity also has improved greatly compared with our previous work [26]. K_{eff}/K_{Cu} is calculated by Eq. (5) as follows :

$$\frac{K_{eff}}{K_{Cu}} = \frac{R_{Cu}}{R} \tag{5}$$

where K_{eff} is the effective thermal conductivity of UTFHP, K_{Cu} is the thermal conductivity of copper, and R_{Cu} is the thermal resistance of the same-sized copper plate.

4. Conclusions

In this study, 0.6 mm thick UTFHPs with novel multiscale concentrated striped composite wick structures are proposed and fabricated. Multiscale micro/nanostructures are prepared on the surface of the wick by alkali-assisted thermal oxidation, and superhydrophilic surfaces are formed. An experimental study on the thermal performance of UTFHPs is carried out. The influence of input heating power, filling ratio, wick configuration, and passage width are analyzed. It is found that the appropriate increment of filling ratio can delay dry-out, reduce temperature difference, and improve the thermal performance of UTFHPs at a high heat load. However, a high filling ratio results in a large thermal resistance. The axially concentrated striped configuration exhibits better thermal performance than the parallel passage configuration. The UTFHP with a hollow and concentrated striped composite wick at the evaporation section has a minimum thermal resistance of 0.79 °C/W at the heating power of 23.34 W, which is about 1/7 of that of the geometrically equivalent copper plate. In addition, the increase in passage width does not improve the thermal performance of UTFHP.

Declaration of competing interest

The authors declare that they have no known competing financial interests or personal relationships that could have appeared to influence the work reported in this paper.

Acknowledgments

This work was supported by the National Natural Science Foundation of China (Grant No. 52076041), the Natural Science Foundation of Jiangsu Province (Grant No. BK20200371), the Zhishan Scholarship of Southeast University (No. 2242022R40037), and the Nanjing Carbon Peak and Carbon Neutrality Science and Technology Innovation Project (Grant No. 202211009).

Nomenclature

FHP	flat heat pipe
UTFHP	ultra-thin flat heat pipe
CSCW	concentrated striped composite wick
HTC	heat transfer capacity
T_e	temperature of the evaporation section (°C)
T_c	temperature of the condensation section (°C)
R	thermal resistance (°C/W)
Q	input heat load (W)
V_l	volume of the filled liquid working medium (cm^3)
V_p	volume of the pores within the wick (cm^3)
K_{eff}	effective thermal conductivity of the UTFHP (W/(m·K))
K_{Cu}	thermal conductivity of the copper (W/(m·K))

Greek symbols

θ	contact angle (°)
η	filling ratio (%)

References

[1] W. Zhou, Y. Li, Z. Chen, L. Deng, Y. Gan, A novel ultra-thin flattened heat pipe with biporous spiral woven mesh wick for cooling electronic devices, Energy Convers. Manag. 180 (2019) 769–783.
[2] Y. Tang, H. Tang, J. Li, S. Zhang, B. Zhuang, Y. Sun, Experimental investigation of capillary force in a novel sintered copper mesh wick for ultra-thin heat pipes, Appl. Therm. Eng. 115 (2017) 1020–1030.
[3] P. Kumar, G. Sahu, D. Chatterjee, S. Khandekar, Copper wick based loop heat pipe for thermal management of a high-power LED module, Appl. Therm. Eng. (2022) 211.
[4] H. Behi, D. Karimi, M. Behi, J. Jaguemont, M. Ghanbarpour, M. Behnia, M. Berecibar, J. Van Mierlo, Thermal management analysis using heat pipe in the high current discharging of lithium-ion battery in electric vehicles, J. Energy Storage 32 (2020).
[5] M. Bernagozzi, A. Georgoulas, N. Miché, M. Marengo, Heat pipes in battery thermal management systems for electric vehicles: a critical review, Appl. Therm. Eng. 219 (2023).
[6] S.H. Moon, K.S. Choi, J.H. Lee, H.T. Kim, Application of aluminum flat heat pipe for dry cooling near the hot spot of a radar array with a multiscale structure, Appl. Therm. Eng. 169 (2020).
[7] Y. Yang, J. Li, X. Ye, H. Qiu, Influence of hydrophobic area fraction of a wettability-patterned evaporator in an ultrathin vapor chamber, Int. J. Heat Mass Tran. (2022) 198.
[8] C. Ding, G. Soni, P. Bozorgi, B.D. Piorek, C.D. Meinhart, N.C. MacDonald, A flat heat pipe Architecture based on nanostructured titania, J. Microelectromech. Syst. 19 (2010) 878–884.
[9] Y. Yang, J. Li, H. Wang, D. Liao, H. Qiu, Microstructured wettability pattern for enhancing thermal performance in an ultrathin vapor chamber, Case Stud. Therm. Eng. 25 (2021).
[10] H. Tang, Y. Tang, Z.P. Wan, J. Li, W. Yuan, L.S. Lu, Y. Li, K.R. Tang, Review of applications and developments of ultra-thin micro heat pipes for electronic cooling, Appl. Energy 223 (2018) 383–400.
[11] C. Oshman, B. Shi, C. Li, R. Yang, Y.C. Lee, G.P. Peterson, V.M. Bright, The development of polymer-based flat heat pipes, J. Microelectromech. Syst. 20 (2011) 410–417.
[12] C. Oshman, Q. Li, L.-A. Liew, R. Yang, V.M. Bright, Y.C. Lee, Flat flexible polymer heat pipes, J. Micromech. Microeng. 23 (2013).
[13] R. Lewis, S. Xu, L.-A. Liew, C. Coolidge, R. Yang, Y.-C. Lee, Thin flexible thermal ground planes: fabrication and scaling characterization, J. Microelectromech. Syst. 24 (2015) 2040–2048.
[14] S. Xu, R.J. Lewis, L.-A. Liew, Y.-C. Lee, R. Yang, Development of ultra-thin thermal ground planes by using stainless-steel mesh as wicking structure, J. Microelectromech. Syst. 25 (2016) 842–844.
[15] D. Lee, C. Byon, Fabrication and characterization of pure-metal-based submillimeter-thick flexible flat heat pipe with innovative wick structures, Int. J. Heat Mass Tran. 122 (2018) 306–314.
[16] G. Huang, W. Liu, Y. Luo, Y. Li, H. Chen, Fabrication and thermal performance of mesh-type ultra-thin vapor chambers, Appl. Therm. Eng. (2019) 162.
[17] Z. Chen, Y. Li, W. Zhou, L. Deng, Y. Yan, Design, fabrication and thermal performance of a novel ultra-thin vapour chamber for cooling electronic devices, Energy Convers. Manag. 187 (2019) 221–231.
[18] H. Li, J. Ren, D. Yin, G. Lu, C. Du, X. Jin, Y. Jia, Effects of inclination angle and heat power on heat transfer behavior of flat heat pipe with bionic grading microchannels, Appl. Therm. Eng. (2022) 206.

[19] G. Huang, W. Liu, Y. Luo, T. Deng, Y. Li, H. Chen, Research and optimization design of limited internal cavity of ultra-thin vapor chamber, Int. J. Heat Mass Tran. 148 (2020), 119101.
[20] W. Zhou, P. Xie, Y. Li, Y. Yan, B. Li, Thermal performance of ultra-thin flattened heat pipes, Appl. Therm. Eng. 117 (2017) 773–781.
[21] L. Lv, J. Li, Managing high heat flux up to 500 W/cm^2 through an ultra-thin flat heat pipe with superhydrophilic wick, Appl. Therm. Eng. 122 (2017) 593–600.
[22] W. Zhou, Y. Li, Z. Chen, L. Deng, Y. Gan, Effect of the passage area ratio of liquid to vapor on an ultra-thin flattened heat pipe, Appl. Therm. Eng. (2019) 162.
[23] J. Li, L. Lv, G. Zhou, X. Li, Mechanism of a Microscale Flat Plate Heat Pipe with Extremely High Nominal Thermal Conductivity for Cooling High-End Smartphone Chips, Energy Conversion and Management, 2019, p. 201.
[24] G. Huang, W. Liu, Y. Luo, Y. Li, H. Chen, A new ultra-thin vapor chamber with composite wick for thin electronic products, Int. J. Therm. Sci. 170 (2021).
[25] Z. Cui, L. Jia, Z. Wang, C. Dang, L. Yin, Thermal performance of an ultra-thin flat heat pipe with striped super-hydrophilic wick structure, Appl. Therm. Eng. (2022) 208.
[26] Y. Yang, D. Liao, H. Wang, J. Qu, J. Li, H. Qiu, Development of ultrathin thermal ground plane with multiscale micro/nanostructured wicks, Case Stud. Therm. Eng. 22 (2020).
[27] R. Wen, S. Xu, Y.-C. Lee, R. Yang, Capillary-driven liquid film boiling heat transfer on hybrid mesh wicking structures, Nano Energy 51 (2018) 373–382.
[28] C. Oshman, Q. Li, L.-A. Liew, R. Yang, Y.C. Lee, V.M. Bright, D.J. Sharar, N.R. Jankowski, B.C. Morgan, Thermal performance of a flat polymer heat pipe heat spreader under high acceleration, J. Micromech. Microeng. 22 (2012).
[29] S.-C. Wong, S.-F. Huang, K.-C. Hsieh, Performance tests on a novel vapor chamber, Appl. Therm. Eng. 31 (2011) 1757–1762.
[30] Z. Sun, X. Chen, H. Qiu, Experimental investigation of a novel asymmetric heat spreader with nanostructure surfaces, Exp. Therm. Fluid Sci. 52 (2014) 197–204.
[31] X. Zhang, Y. Guo, W. Liu, J. Hao, CuO three-dimensional flowerlike nanostructures: controlled synthesis and characterization, J. Appl. Phys. 103 (2008).
[32] R.J. Moffat, Describing the uncertainties in experimental results, Exp. Therm. Fluid Sci. 1 (1988) 3–17.
[33] J. Li, L. Lv, Experimental studies on a novel thin flat heat pipe heat spreader, Appl. Therm. Eng. 93 (2016) 139–146.
[34] Y. Li, J. He, H. He, Y. Yan, Z. Zeng, B. Li, Investigation of ultra-thin flattened heat pipes with sintered wick structure, Appl. Therm. Eng. 86 (2015) 106–118.